fire

MDPI

Article

Study on the Synergistic Spontaneous-Combustion Effects and Critical Behavior of Polyurethane and Residual Coal Based on Large-Scale Programmed Heating Tests

Yu Wang [1], Baoshan Jia [2,3,4], Zikun Pi [5,*], Rui Li [5], Tianzhi Yang [2,3], Zhanpeng He [5], Hui Zhuo [6] and Tongren Li [6]

[1] Shanxi Lu'an Mining Group Co., Ltd., Changzhi 046200, China
[2] School of Safety Science and Engineering, Liaoning Technical University, Huludao 125105, China
[3] Key Laboratory of Mine Thermodynamic Disaster Prevention and Control, Ministry of Education, Huludao 125105, China
[4] Key Laboratory of Coal Mine Fire and Gas Prevention and Control, State Mine Safety Supervision Bureau, Fushun 113000, China
[5] School of Safety and Management Engineering, Hunan University of Technology, Hengyang 421002, China
[6] School of Safety Science and Engineering, Anhui University of Science and Technology, Huainan 232001, China; zhuohui1130@aust.edu.cn (H.Z.)
* Correspondence: 2025100047@aust.edu.cn; Tel.: +86-18361276826

Abstract

To address the major safety hazard that heat released from mining polyurethane (PU) reinforcement materials may induce spontaneous combustion of residual coal in goaf, this study selected No. 3 coal from Wangzhuang Coal Mine, Shanxi Lu'an, as the research object. A self-developed large-capacity, large-scale experimental system was used to conduct programmed heating experiments on 2.0 kg multi-particle-size coal-PU mixed samples. The effects of PU content on characteristic gas release, crossing point temperature (CPT), residue morphology, and TGA-DSC characteristic temperatures were systematically investigated, and the reaction-kinetic evolution was further analyzed using the distributed activation energy model (DAEM). The results show that coal and PU exhibit a significant synergistic enhancement effect during co-heating. As the PU content increased, the release concentrations of CO, C_2H_4, and C_2H_6 increased markedly, and their initial release temperatures decreased, whereas CH_4 generation was inhibited by hydrogen-radical competition; no C_2H_2 was produced below 400 °C. The CPT decreased linearly with an increasing PU content, with an average decrease of approximately 8.5 °C for every 10% increase in PU content. Residue morphology showed clear critical features: glassy agglomerates appeared when the PU content exceeded 16.67%, and dense bulk coking occurred when the PU/coal mass ratio was greater than 1:10. TGA-DSC analysis showed that when the PU/coal ratio was lower than 1:10, the ignition temperature of the mixed sample was higher than that of pure coal, indicating an inhibitory synergistic effect. When the ratio exceeded 1:10, the ignition temperature decreased significantly, and the synergy shifted to promotion; increasing the heating rate shifted the characteristic temperatures to higher values and increased the reaction intensity. DAEM analysis further confirmed that when the PU ratio exceeded 1:10, the apparent activation energy of the mixed samples was lower than that of pure coal. Coal powder also acted as a physical skeleton that effectively dispersed molten PU, eliminated the activation-energy peaks of pure PU in the conversion ranges of 30–50% and 70–90%, and substantially improved combustion stability. Mechanistically, low-temperature PU melting and coating optimized heat and mass transfer, medium-temperature pyrolysis released active radicals and combustible gases that altered coal pyrolysis pathways and the radical reaction environment, and high-temperature hydrogen-radical competition reshaped the gas-product distribution. Together, these processes form a complete chain of

Check for updates

Academic Editor: Quanlin Shi

Received: 30 May 2026
Revised: 30 June 2026
Accepted: 2 July 2026
Published: 7 July 2026

Copyright: © 2026 by the authors. Licensee MDPI, Basel, Switzerland. This article is an open access article distributed under the terms and conditions of the Creative Commons Attribution (CC BY) license.

synergistic spontaneous combustion. This study identifies key safety threshold parameters for PU reinforcement materials, recommends a PU content of ≤9.10%, and identifies CO and C_2H_4 as priority early-warning gases, providing direct experimental evidence for characteristic-gas-based early warning and mine fire prevention.

Keywords: polyurethane reinforcement; residual coal; programmed heating; spontaneous ignition; fire safety; crossing point temperature

1. Introduction

Coal remains a major industrial energy source and accounts for a substantial share of global energy consumption [1]. Spontaneous combustion of coal is a persistent safety challenge in underground mining [2]. Polymer grouting can improve the structural stability of coal walls and roofs, reduce potential hazards, and protect workers during mine production [3]. Polyurethane (PU) reinforcement material is a polymer produced by the reaction between isocyanate groups (R-NCO) and polyols (R′-OH). Owing to its molecular structure, PU exhibits a high compressive strength, favorable mechanical performance, and good weather resistance [4]. The use of PU for coal and rock reinforcement was tested in China as early as February 1982, when Kailuan Fangezhuang Mine and Bayer jointly conducted field trials and obtained favorable results [5]. In recent years, polymer reinforcement materials have been widely applied in coal mines. PU can fill and bond fractures and voids in coal and rock, reinforce the coal body, and improve its compressive resistance, thereby helping to prevent rock fracturing, roof collapse, and related mine accidents [6]. In working faces, PU-based coal-wall reinforcement is commonly combined with support advancement under a load and timely roof support to control rib spalling and roof falls. However, the interaction between PU and coal releases heat. As a result, the field application of polymer reinforcement materials can introduce secondary hazards, including smoke generation, overheating, combustion, and excessive carbon monoxide concentrations. These hazards pose a serious threat to the stability of coal mine safety production [7].

In response to these problems, many studies have examined the safe use of PU materials in underground mines. Xu et al. [8] reported that underground fires associated with PU mainly arise from two mechanisms: direct self-ignition of PU after contact with oxygen at high temperature, and indirect ignition of coal seams caused by heat released during PU combustion. Wang et al. [9] conducted TGA-DSC programmed heating experiments on three coal samples with different metamorphic degrees and found that coal combustion characteristic parameters were positively correlated with the heating rate and negatively correlated with the coal metamorphic degree. Yang et al. [10] investigated the oxidation behavior of five particle-size fractions of coal using a programmed heating system and found that apparent activation energy increased with the particle size. The particle size was positively associated with the minimum thickness of loose coal and the lower limit of the oxygen volume fraction, but negatively associated with the upper limit of air leakage intensity. Wang et al. [11] examined the spontaneous-combustion kinetics and gas-release behavior of a coal-PU binary system by thermogravimetric analysis and spontaneous-combustion simulation experiments. They found that a higher PU mass fraction lowered the release temperatures of CO_2, CO, C_2H_6, and C_2H_4; the release amounts of CO_2, CO, and C_2H_6 increased with the PU content, whereas C_2H_4 showed the opposite trend. Ye et al. [12] combined FTIR and programmed heating experiments and found that aromatic hydrocarbons increased, oxygen-containing functional groups decreased, and characteristic temperatures increased with an increasing coal metamorphic degree.

Tang et al. [13] performed adiabatic oxidation and TG-DTG analyses and found that PU showed pronounced pyrolysis behavior during combustion of coal-PU mixed samples. Tian et al. [14] investigated gas release during spontaneous combustion of PU-coal mixtures, the evolution of PU spontaneous combustion in goaf, and the migration of generated gases through experiments, chemical analysis, and numerical simulation. Wang et al. [15,16] demonstrated a synergistic effect between coal and PU during combustion, with inhibition at coal-to-PU ratios lower than 1:15 and promotion at ratios higher than 1:15.

Research on PU use and flame-retardant modification in coal mines has also been conducted from the perspectives of grouting technology [17–19], surface-modified coal gangue powder (MCG) [20], expandable graphite (EG) and dimethyl methyl phosphonate (DMMP) [21], reduced graphene oxide/polyaniline (rGO/PANIf) [22], and formulation optimization [23–26]. Gao et al. [27] prepared a microencapsulated diatomite-supported flame retardant (MDFR), which improved the mechanical performance, preserved the cellular structure, and enhanced the thermal stability of mining rigid polyurethane foam compared with conventional flame retardants such as DMMP and tris(2-chloropropyl) phosphate. Wang [28] analyzed the mechanism by which resin heat release causes fire and proposed prevention strategies. Yang et al. [29] used an L9(3^4) orthogonal experiment to determine an optimal formulation that balanced flame retardancy and compressive performance. Cheng et al. [30] found that cement incorporation improved the flame-retardant performance of resin materials. Wang et al. [31] developed rigid PU foam synergistically modified with expandable graphite, melamine phosphate, and 2-carboxyethyl(phenyl)phosphinic acid, effectively improving the flame-retardant grade. Ma et al. [32] studied the fire risk of rigid PU foam under high-pressure, low-oxygen conditions and identified oxygen reduction as a key factor for controlling combustion intensity. Chen et al. [33] investigated the effect of sample thickness on thermoplastic PU combustion behavior. Ren et al. [34] summarized fire risks and countermeasures during resin foam storage and use. Zhang [35] reduced the maximum reaction temperature below 100 °C and achieved compressive strength above 40 MPa by optimizing catalyst-to-main-agent ratios. Zhang et al. [36] established a gas-release model for coal-resin co-combustion and confirmed that resin addition can reduce the CPT of mixed samples.

Overall, existing studies have provided detailed insights into coal spontaneous combustion and the thermodynamic interaction between coal and PU. However, most experiments have used small-mass, single-particle-size samples, which differ substantially from the large-volume, multi-particle-size residual coal environment in underground mines. The formation behavior of high-temperature gas products and the critical disaster-triggering conditions remain to be clarified systematically. Therefore, this study used 2.0 kg large-scale multi-particle-size mixed samples to simulate the actual particle-size distribution of underground coal. Programmed heating experiments were conducted to analyze the effects of PU content on gas release, CPT, and residue morphology, and key critical parameters were identified to provide an experimental basis for the safe underground application of polymer materials and fire prevention.

2. Materials and Methods

2.1. Preparation of Coal and Polyurethane Samples

To accurately characterize the spontaneous-combustion behavior of residual coal in goaf induced by heat released from PU, No. 3 coal from the Wangzhuang Coal Mine of Shanxi Lu'an was selected as the test coal. After removal of the surface oxidized layer, the coal was crushed and sieved into six particle-size fractions, which were then mixed according to field proportions. The particle-size fractions and corresponding mass percentages are listed in Table 1.

Table 1. Particle size distribution and mass fraction of coal samples.

Particle Size of Coal Sample/mm	<1	1~3	3~5	5~10	10~20	20~30
Mass Fraction/%	10	10	20	25	25	10

The PU reinforcement material (Shanxi Lu'an Jin'an Mining Engineering Co., Ltd., Changzhi, Shanxi, China) used in the experiments was a two-component system. Component A was a polyether polyol blend, and Component B was a polymeric MDI system. The two components were mixed at a mass ratio of 1:1 and cured to form a nonfoaming, dense solid. The cured PU was then crushed, sieved, and blended according to the particle-size distribution shown in Table 2.

Table 2. Polyurethane particle size distribution and mass fraction.

PU Particle Size/mm	<1	1~3	3~5	5~10	10~20
Mass Fraction/%	5	10	20	25	40

During programmed heating, PU particles in the 20–30 mm fraction are prone to delayed internal pyrolysis, surface melting and coating, and delayed gas release, which can reduce data accuracy. Considering the particle-size distribution commonly used in large-particle coal spontaneous-combustion experiments, the 10–20 mm fraction was selected instead because it better represents large bulk materials underground while ensuring sufficient heat transfer and relatively uniform pyrolysis. Preliminary experiments confirmed that this substitution had no significant effect on the pyrolysis behavior or gas-release pattern of PU [10,37].

2.2. Experimental Scheme

2.2.1. Large-Scale Programmed Heating Experiment

Eight sample groups were prepared with different coal-to-PU mass ratios, and each group had a total mass of 2.0 kg. The specific mixing proportions are listed in Table 3.

Table 3. Composition of experimental samples.

Sample Number	Proportioning (PU: Coal)	PU Content/%
C	0:1	0
P-C-1	1:30	3.26
P-C-2	1:20	4.76
P-C-3	1:10	9.1
P-C-4	1:5	16.67
P-C-5	1:3	25
P-C-6	1:1	50

Each sample was mixed at 90 r/min for 10 min to ensure homogeneity, dried at 105 °C to a constant mass, and then loaded into the coal reaction vessel. During loading, layered vibration compaction was used, with each 5 cm coal layer vibrated for 30 s, to reduce porosity heterogeneity caused by local accumulation of fine particles. A porous ceramic distributor plate with a pore size of 2–3 mm and a thickness of 1 cm was installed at the bottom of the furnace to improve gas-flow uniformity. Synthetic air, consisting of 21% O_2 and 79% N_2, was used as the experimental atmosphere. The heating program was staged: the temperature was increased from 20 °C to 150 °C at 0.5 K/min and from 150 °C to 400 °C at 1 K/min. The inlet gas flow rate was set to 80 mL/min from 20 °C to 200 °C and 120 mL/min from 200 °C to 400 °C. Each experiment was performed in triplicate, and

average values were used; the relative error was less than 5%. The gas chromatograph was a Beijing Purui GC7800A (Beijing Purui Analytical Instruments Co., Ltd., Beijing, China), and the temperature recorder was a Changzhou Haierpa HPS3032 multi-channel temperature tester (Changzhou Haierpa Electronic Technology Co., Ltd., Changzhou, China). The programmed heating and gas chromatography experimental system is shown in Figure 1, and photographs of the coal reaction vessel and electrothermal blast drying oven are shown in Figure 2.

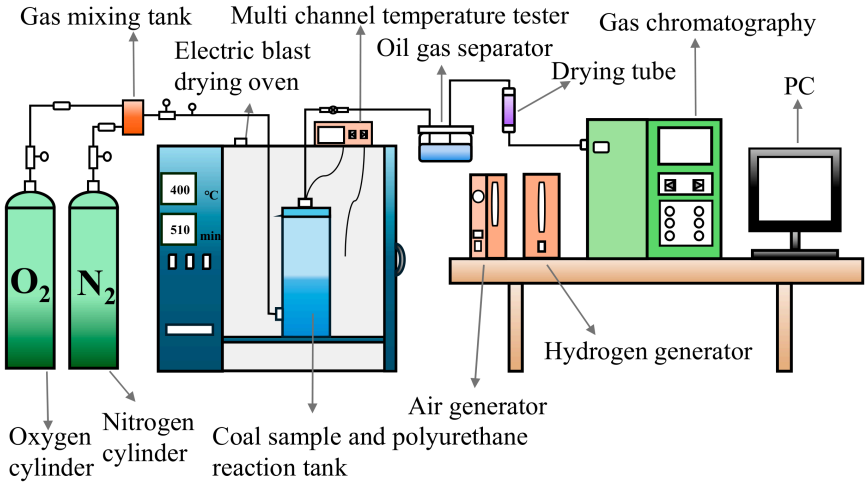


Figure 1. Schematic diagram of the programmed heating and gas chromatography experimental system.



Figure 2. Photographs of the coal reaction vessel and electrothermal blast drying oven.

2.2.2. TGA-DSC Test

To investigate the synergistic or inhibitory effect between coal and PU during co-pyrolysis, eight mixed samples with different mass ratios were prepared, as shown in Table 3. For each test, 10 mg of sample was used. Thermogravimetric analysis was performed at three heating rates (5, 10, and 20 K/min) over the temperature range of 30–800 °C in an air atmosphere consisting of 79% N_2 and 21% O_2.

2.3. Experimental Test

After the outlet gas was passed through a saturated $NaHCO_3$ solution to remove tar and then dried with silica gel, the concentrations of CO, CH_4, C_2H_4, C_2H_6, and C_2H_2 were measured using a ZRD-II coal spontaneous-combustion characteristic tester and a

gas chromatograph. The temperature inside the reactor and the furnace temperature were recorded using a multichannel temperature recorder to determine the CPT. In this study, the initial release temperature of each characteristic gas was defined as the central temperature of the reaction vessel when the gas concentration first remained above the chromatograph detection limit (CO $\leq$ 1 ppm; hydrocarbons $\leq$ 0.5 ppm) and subsequently showed a monotonic increasing trend. The average value from parallel experiments was used.

3. Results and Analysis

3.1. CO Release Behavior

The CO release pattern during spontaneous combustion of the mixed samples is shown in Figure 3. For the pure coal sample, the CO concentration increased rapidly above 200 °C and reached 4843 ppm at 400 °C. As the PU content increased, the initial CO release temperature decreased and the CO concentration increased. For sample PC6, the CO concentration rose sharply above 280 °C and reached 15,340 ppm at 400 °C. This increase may be attributed to PU pyrolysis, which promotes the decomposition of oxygen-containing functional groups in coal. In addition, PU melting and coating increased the effective reaction surface area, thereby markedly enhancing the CO release rate.

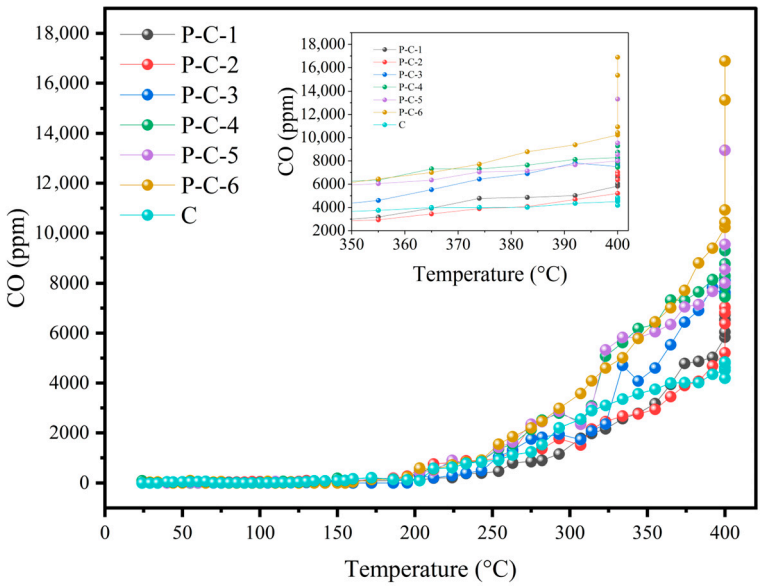


Figure 3. CO gas release pattern during spontaneous combustion of mixed samples.

As shown in Figure 3, when the temperature reached approximately 200 °C, isocyanate began to decompose into amine compounds (R-NH_2) and other by-products, and CO was released slowly. PU is produced by the reaction between polyols (R-OH) and isocyanates (R-N=C=O), and its thermal decomposition can interact with coal oxidation during co-combustion. Between 280 °C and 350 °C, thermal activation promoted the cleavage of C-C bonds in aldehyde groups (R-CHO) and the removal of carbonyl groups (-C=O), generating R-H species with one fewer carbon atom and CO; consequently, the CO concentration gradually increased. Above 350 °C, the synergistic decomposition of oxygen-containing functional groups in coal became more pronounced, leading to a sharp increase in CO concentration. In addition, PU melted and coated the coal particles during heating. With increasing temperature, coal particles became more fragmented, cracks developed, and oxygen diffusion was enhanced. These changes increased the contact area between PU and coal and expanded the effective reaction zone, thereby promoting CO generation and release.

3.2. CH_4 Release Behavior

The CH_4 release pattern during spontaneous combustion of the mixed samples is shown in Figure 4. For the pure coal sample, the CH_4 concentration reached a peak of 3592 ppm at 355 °C and then decreased to 1970 ppm at 400 °C. PU inhibited CH_4 generation: as the PU content increased, the peak CH_4 concentration decreased and the release peak shifted to a higher temperature. For sample PC6, the CH_4 concentration reached only 372.4 ppm at 390 °C. This inhibition can be attributed to the molten coating layer formed by a high PU content, which restricted the cleavage of aliphatic side chains and the escape of CH_4.

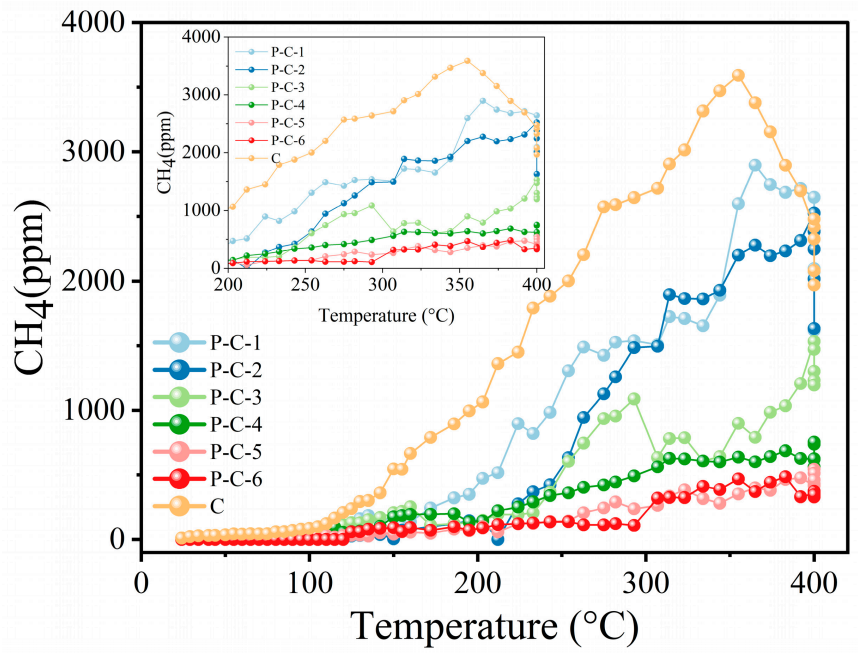


Figure 4. CH_4 gas release pattern during spontaneous combustion of mixed samples.

In the mixed samples, aliphatic side chains in coal molecules began to cleave above 250 °C and generated CH_4 through free-radical reactions. As the PU proportion increased, the amount of CH_4 released decreased. This decrease occurred because CH_4 was mainly generated from the cleavage of methyl groups in coal. Although PU can produce hydrocarbon gases during combustion, it lacks a reaction pathway for the formation of stable alkanes. In addition, a high PU proportion promoted the formation of large molten agglomerates at a high temperature. These agglomerates not only impeded CH_4 release but also caused PU and coal particles to bind together, thereby further suppressing CH_4 generation.

More importantly, PU and coal differ fundamentally in their pyrolysis chemistry. Active intermediates generated during PU pyrolysis strongly compete for hydrogen radicals (H·). PU pyrolysis mainly produces oxygen-containing gases and olefins, and the highly reactive free radicals formed in this process compete with methyl radicals generated from coal pyrolysis for available hydrogen sources. At the reaction pathway level, this competition suppresses the key chain-termination step responsible for CH_4 formation during coal pyrolysis ($\cdot CH_3 + H\cdot \rightarrow CH_4$), thereby chemically inhibiting the methane generation pathway. In addition, the early decomposition and molten state of PU may promote secondary reactions involving methane, further reducing its apparent release concentration.

3.3. C_2H_4 and C_2H_6 Release Behavior

The release patterns of the indicator gases C_2H_4 and C_2H_6 during spontaneous combustion of the mixed samples are shown in Figures 5 and 6. In the pure coal sample, the

release amounts of C_2H_4 and C_2H_6 were extremely low. As the PU content increased, the concentrations of both gases increased markedly. For sample P-C-6, the concentrations of C_2H_4 and C_2H_6 reached 3472 ppm and 90.17 ppm, respectively, at 400 °C.

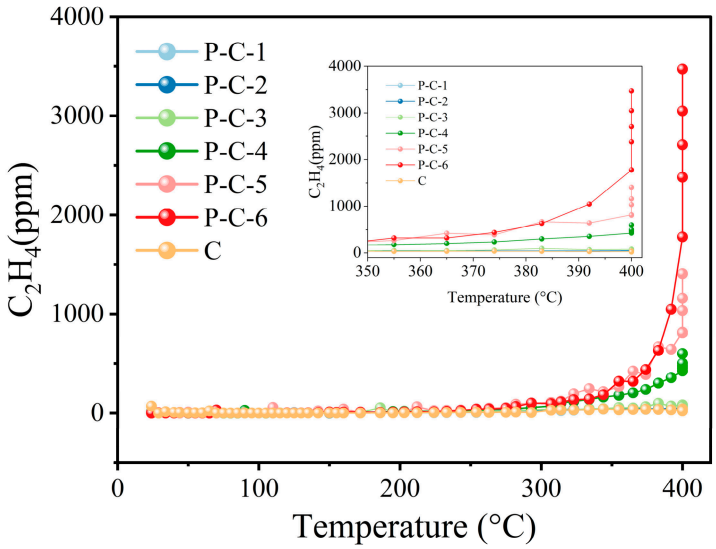


Figure 5. C_2H_4 gas release pattern during spontaneous combustion of mixed samples.

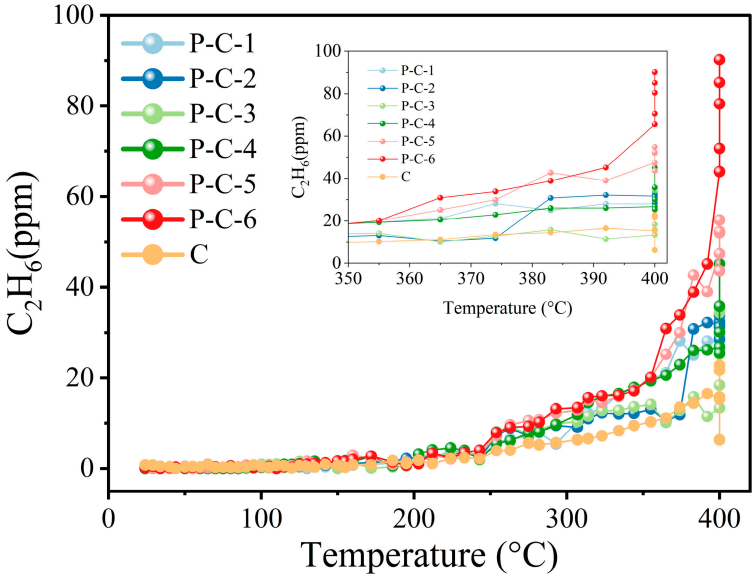


Figure 6. C_2H_6 gas release pattern during spontaneous combustion of mixed samples.

The sharp increase in C_2H_4 and C_2H_6 concentrations with an increasing PU content can be attributed to the combined effects of direct gas generation from PU and PU-induced enhancement of coal degradation pathways. This behavior indicates a pronounced synergistic effect in the coal-PU mixed system during thermal oxidation and suggests that PU can accelerate coal spontaneous combustion.

3.4. C_2H_2 Release Behavior

The C_2H_2 release pattern during spontaneous combustion of the mixed samples is shown in Figure 7. C_2H_2 was not detected in either the pure coal sample or the coal-PU mixed samples, indicating that PU did not directly generate C_2H_2 under the experimental conditions. In PU, polymeric MDI reacts with polyols to form urethane bonds containing benzene-ring structures. Below 400 °C, these benzene-ring-containing urethane bonds

mainly decompose into amines, CO, and CO_2, while ether-bond cleavage primarily generates C_2H_6. In addition, the aliphatic chains in coal are relatively short and do not provide sufficient long-chain hydrocarbon precursors for C_2H_2 formation below 400 °C. Therefore, the conditions required for C_2H_2 generation were not reached in this temperature range.

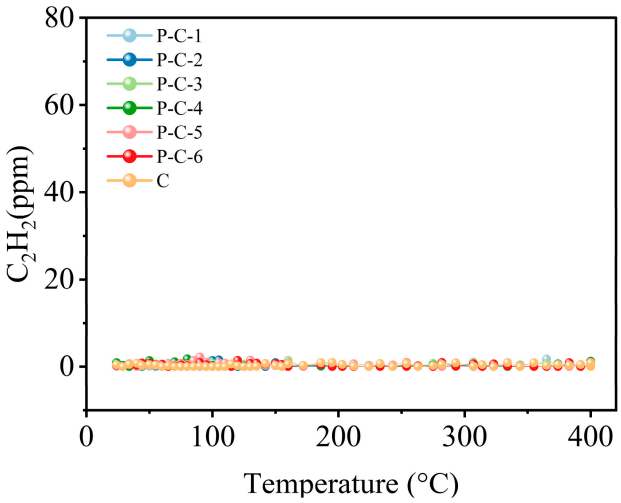


Figure 7. C_2H_2 gas release pattern during spontaneous combustion of mixed samples.

3.5. Temperature Trend and CPT Analysis During Spontaneous Combustion

The temperature trends during spontaneous combustion of the coal and mixed samples are shown in Figure 8.

The CPT is the critical temperature at which the self-heating rate of the sample exceeds the programmed heating rate, and it directly reflects the susceptibility of the sample to spontaneous combustion. As shown in Table 4, the CPT decreased and occurred earlier as the PU content increased. The CPT of the pure coal sample was 231.6 °C, whereas that of PC6 decreased to 199.9 °C. On average, each 10% increase in PU content reduced the CPT by 8.5 °C. Below 150 °C, samples with a lower PU proportion showed a slower temperature increase. This stage was dominated by endothermic processes, mainly moisture loss from coal, and the sample temperature lagged behind the furnace temperature. Above 150 °C, the increased inlet gas flow accelerated the temperature rise inside the reactor, intensified coal–oxygen complex exothermic reactions, and enhanced the oxidation heat release of volatile compounds, leading to the turning point marked by the CPT.

Table 4. CPT values during spontaneous combustion of coal and mixed samples.

Sample Number	CPT/°C	CPT Occurrence Time/Min
C	231.6	480
P-C-1	213.9	440
P-C-2	210.5	430
P-C-3	208.7	430
P-C-4	208.6	430
P-C-5	204.7	420
P-C-6	199.9	410

The decrease in CPT was mainly caused by the synergistic interaction between PU and coal. PU pyrolyzed at a relatively low temperature and generated abundant volatile and combustible gases, which rapidly oxidized and released heat. This process initiated the coal–oxygen self-heating reaction earlier, causing coal to participate in oxidation at a temperature lower than its intrinsic ignition temperature.

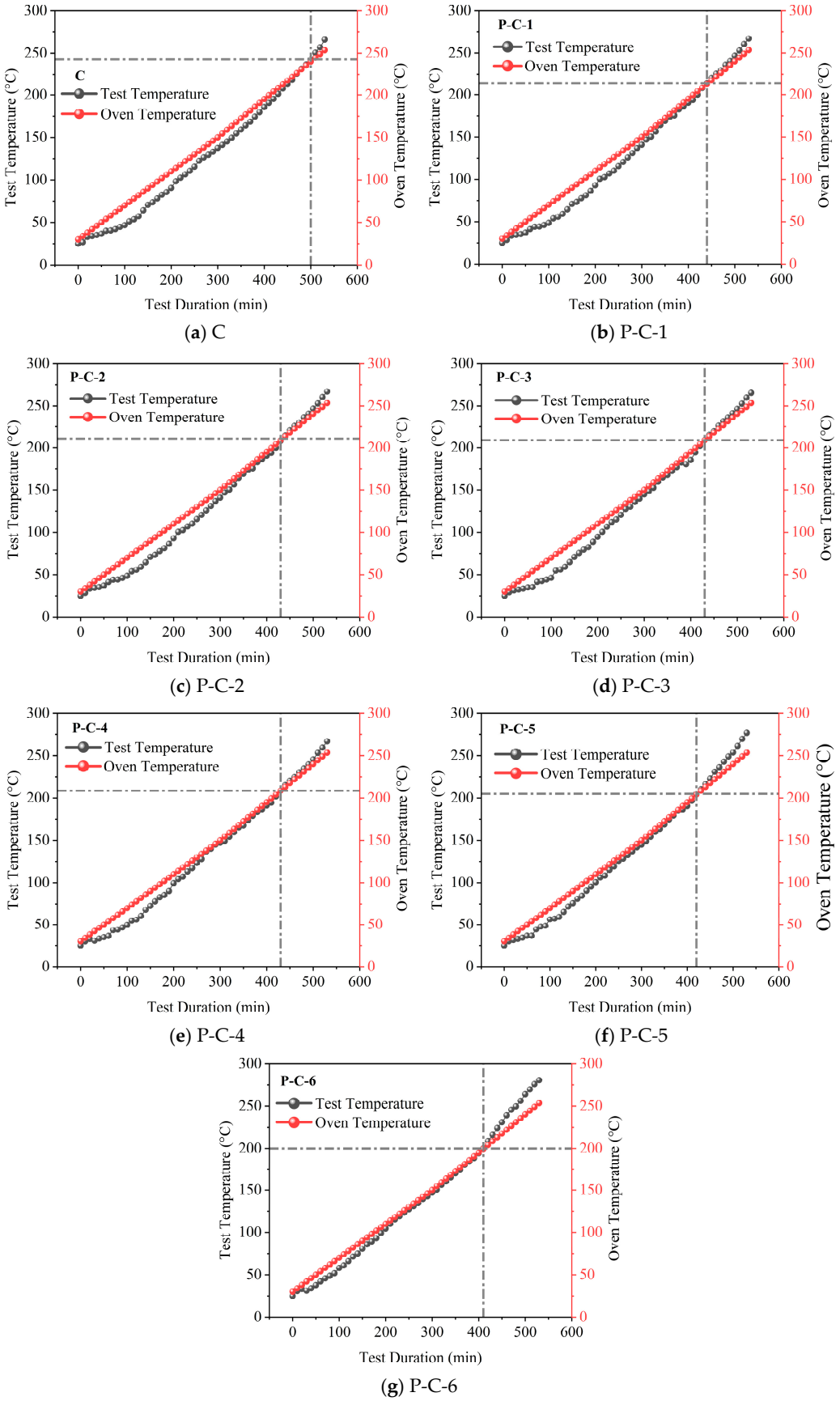


Figure 8. Temperature trends during spontaneous combustion of coal and mixed samples.

3.6. Surface Morphology Before and After Combustion

The surface morphology of the pure coal sample before and after combustion and that of the mixed samples after combustion are shown in Figure 9.

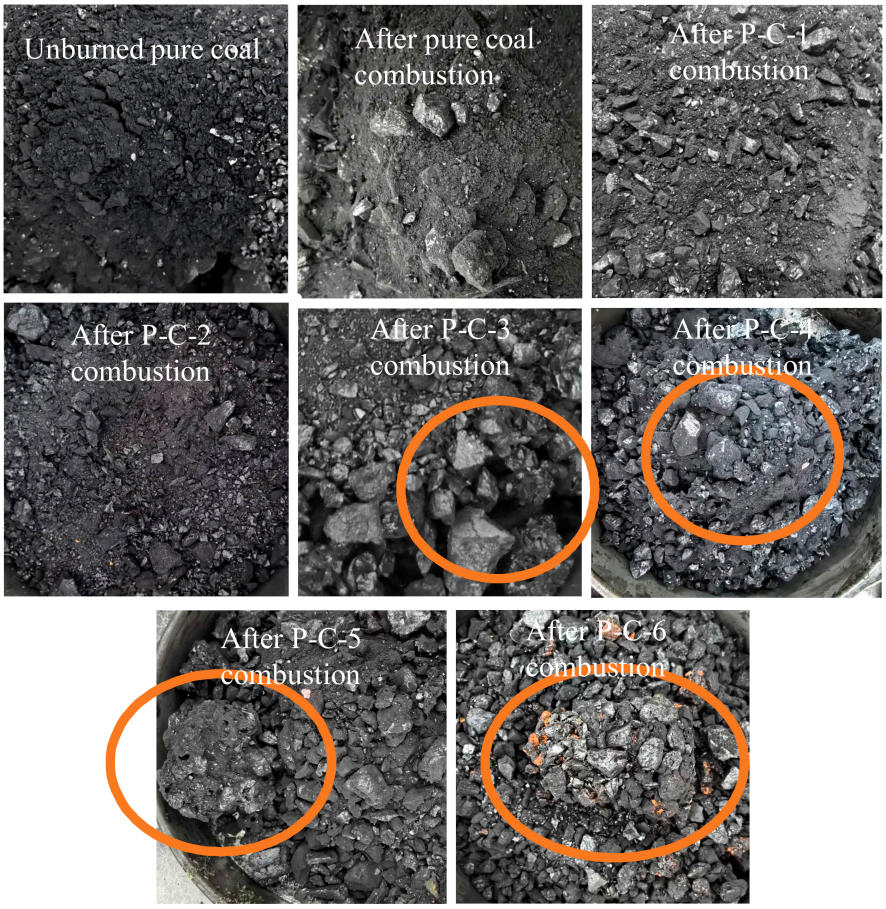


Figure 9. Surface morphology of the pure coal sample before and after combustion and of mixed samples after combustion.

Before combustion, the pure coal surface was mostly dark black and glossy. After combustion, the loose residue on the coal surface consisted of fine particles similar to coal ash and was mainly gray–black. In the mixed samples, a higher PU content led to larger agglomerates in the post-combustion residue and a more consolidated overall structure.

When the PU content was below 9.10%, the residue mainly consisted of coal slag, with no clear agglomeration. When the PU content reached 16.67%, glassy and glossy lumps appeared on the residue surface. When the mass ratio exceeded 1:10, the entire residue showed coking characteristics and formed a dense, hard structure. At a high temperature, PU melted and infiltrated coal fissures, bonding coal particles and forming a ceramic-like bridging phase. Upon cooling, this phase solidified into a strong coke-like mass.

3.7. TGA-DSC Results and Combustion Kinetic Analysis of Mixed Samples

TGA-DSC tests were conducted on mixed samples with different proportions. The TG-DTG curves obtained at a heating rate of 5 K/min are shown in Figure 10. The combustion characteristic temperatures of samples with different proportions at different heating rates are listed in Table 5.

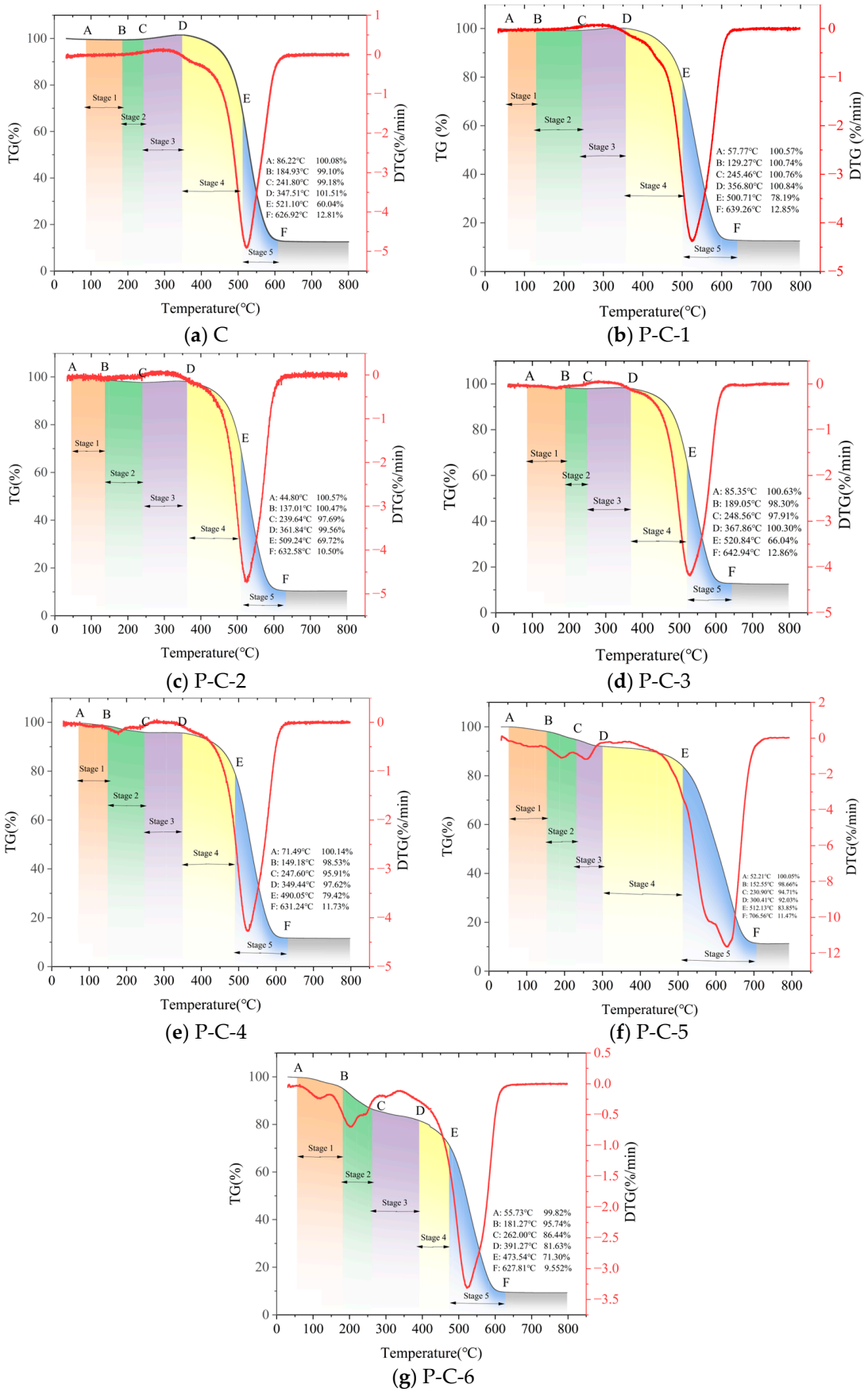


Figure 10. TG-DTG curves of mixed samples with different proportions at a heating rate of 5 K/min.

Table 5. Combustion characteristic temperatures of mixed samples with different proportions at different heating rates.

Characteristic Temperature	Heating Rate (K/min)	Mixed Samples in Different Proportions						
		C	P-C-1	P-C-2	P-C-3	P-C-4	P-C-5	P-C-6
Ti	5	462.2	467.3	464.4	451.2	438.5	420.2	175.4
	10	482.4	485.2	483.5	462.3	448.7	422.1	188.5
	20	492.2	498.5	495.3	478.1	465.4	438.1	208.2
Tb	5	626.9	639.3	632.6	642.9	631.2	633.5	634.8
	10	655.2	654.5	653.1	640.8	665.4	658.7	652.3
	20	710.4	730.1	715.6	720.5	728.8	715.2	715.6
Tmax	5	538.5	535.2	532.5	528.4	525.1	535.2	535
	10	558.6	552.4	562.7	548.1	575.2	556.5	595.4
	20	582.5	646.2	577.1	631.5	635.8	628.4	634.2
DTGmax	5	−4.6	−4.1	−4.6	−4.3	−4.2	−4.1	−3.4
	10	−6.3	−7	−6.7	−6.6	−5.8	−6.8	−6.2
	20	−11.8	−10.4	−12.2	−12.9	−12.1	−11.4	−9.3

According to Figure 10 and Table 5, the ignition temperature of the pure coal sample (C) was higher than that of P-C-3 to P-C-6 (1:10 to 1:1), but lower than those of P-C-1 (1:30) and P-C-2 (1:20). When the PU/coal ratio reached 1:10, the ignition temperature of the mixed samples decreased sharply, and the synergistic effect was enhanced. When the PU/coal ratio was lower than 1:10, the ignition temperature of the mixed samples was higher than that of pure coal, indicating inhibition. When the ratio exceeded 1:10, the ignition temperature was lower than that of pure coal, indicating promotion. At a heating rate of 5 °C/min, the ignition temperature of pure coal was 462.2 °C, whereas that of P-C-6 decreased sharply to 175.4 °C. This behavior is related to the degradation of many unstable chemical bonds in PU at high temperature, which generates volatiles and releases heat. As the heating rate increased, the characteristic temperatures of the mixed samples shifted overall to higher temperature ranges, and the reaction intensity per unit time increased, with a significant increase in maximum mass-loss rate (DTGmax). Differences in molecular structure and thermal stability between coal and PU changed the reaction mechanism of the mixed fuel from concentrated heat release by a single component to staged combustion of multiple components across temperature ranges, effectively decoupling low-temperature ignition from high-temperature burnout.

It should be noted that the DAEM model is strictly based on the assumption of a first-order pyrolysis reaction under an inert atmosphere. In this study, DAEM was applied to combustion TGA-DSC data obtained in air mainly as a mathematical approximation to compare the evolution trends of apparent activation energy among different mixed samples, rather than to obtain intrinsic kinetic parameters with absolute physical meaning. Therefore, the analysis emphasizes relative trends, and the absolute values should be interpreted cautiously in connection with the reaction mechanism. Based on DAEM, the apparent activation energy of coal-PU mixed samples during combustion was calculated and analyzed, and the variation trend is shown in Figure 11.

As shown in Figure 11, the apparent activation energy of pure coal (C) first increased and then decreased with conversion. When 5% < α < 40%, the apparent activation energy increased within the range of 130.6–140.7 kJ/mol and reached 140.5 kJ/mol at α = 5%. When 40% < α < 95%, the apparent activation energy fluctuated downward within the range of 106.5–125.6 kJ/mol and reached the minimum value of 106.5 kJ/mol at α = 95%. This evolution reflects the complex multi-stage combustion behavior of coal. In the early stage (α < 40%), aliphatic side chains (-CH_3 and -CH_2-) and oxygen-containing functional groups, including hydroxyl (-OH), carboxyl (-COOH), and carbonyl (-C=O), preferentially

cleaved and oxidized. Breaking these functional groups required overcoming moderate energy barriers, causing the activation energy to increase as the reaction proceeded [38]. In the middle and late stages (α > 40%), macromolecular aromatic nuclei in coal began to undergo condensation and oxidation. However, because many active functional groups had already been consumed and pore structures had formed, oxygen diffusion and reaction accessibility improved, leading to a downward trend in apparent activation energy [39].

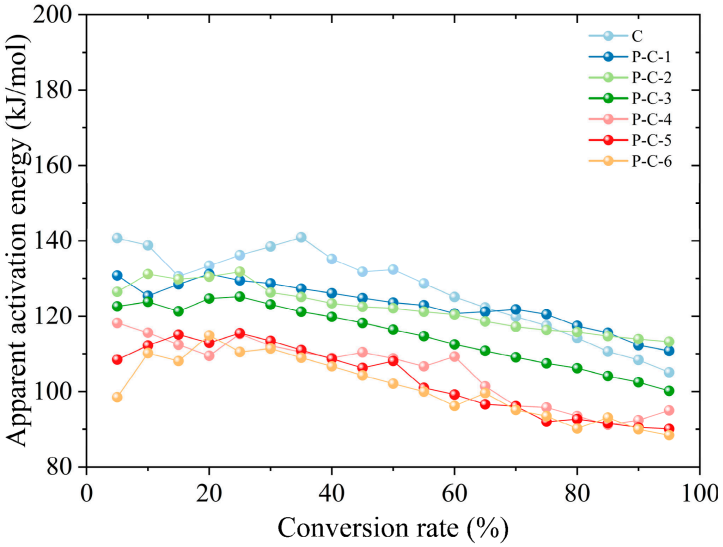


Figure 11. Variation trend of apparent activation energy of coal-PU mixed samples based on the DAEM model.

In the first stage (5% < α < 45%), the activation energy increased continuously from 95.2 to 196.7 kJ/mol and reached a peak at α = 45%. This stage corresponds to cleavage of thermally less stable urethane bonds in PU molecules. The C-O bond in urethane groups (-NH-COO-) begins to break at 170–200 °C, generating isocyanates and polyols, which further decompose into amines, olefins, and CO_2. As the reaction proceeds, the chemical environment of the remaining urethane groups becomes more stable, for example, through protection by adjacent benzene-ring conjugation, requiring higher energy for bond cleavage and leading to the activation-energy peak of 196.7 kJ/mol.

In the second stage (50% < α < 65%), the activation energy decreased sharply from 175.1 to 124.3 kJ/mol, reaching the minimum value of this interval at α = 65%. This stage corresponds to intense oxidative release of volatiles. Isocyanate and polyol fragments generated by earlier urethane-bond cleavage decomposed rapidly as temperature increased, releasing small molecules such as CO, CO_2, and olefins. The release of these volatile products involved a lower energy barrier, and the pore structure formed during earlier reactions improved mass transfer, jointly causing a marked decrease in apparent activation energy.

In the third stage (70% < α < 80%), the activation energy increased again from 133.4 to 151.2 kJ/mol and reached a peak at α = 80%. This stage corresponds to cleavage of the more stable ether bonds (-C-O-C-) in the polyether polyol backbone of PU and oxidation of the residual carbon skeleton. Ether bonds have a higher bond energy than urethane bonds and therefore require higher activation energy for cleavage. In addition, benzene-ring structures in PU begin oxidative ring-opening reactions in this stage, further increasing activation energy.

In the fourth stage (85% < α < 95%), the activation energy decreased again to 118.1 kJ/mol. This stage corresponds to deep oxidation and burnout of residual carbon. The reactants became more homogenized, and the pore structure formed during

earlier reactions allowed more sufficient oxygen diffusion, causing the activation energy to continue decreasing.

For the mixed samples (P-C-1 to P-C-6), during the stage of 5% < α < 40%, when the PU/coal ratio was lower than 1:10, the apparent activation energy of the mixed samples was higher than that of pure coal, indicating an inhibitory synergistic effect. When the PU/coal ratio was higher than 1:10, the apparent activation energy of the mixed samples was lower than that of pure coal, indicating a promoting synergistic effect. With an increasing PU proportion, the apparent activation energy showed an overall decreasing trend.

4. Mechanism of the Coal-PU Synergistic Spontaneous-Combustion Effect

Based on the experimental results presented above, the thermal interaction between coal and PU during programmed heating is not a simple superposition of their individual effects. Instead, coal and PU exhibit a pronounced synergistic effect that intensifies coal spontaneous combustion. The mechanism of this synergistic spontaneous-combustion effect is illustrated in Figure 12. This effect extends throughout the process from low-temperature oxidation to high-temperature pyrolysis. Essentially, the introduction of PU systematically alters the self-heating and combustion behavior of coal through two coupled pathways: physical heat and mass transfer, and the chemical reaction network.

(1) Low-temperature melting (<200 °C). At relatively low temperatures, approximately 150–200 °C, PU first softens and melts, forming a viscous liquid phase. This liquid phase wets and coats coal particles, forming a continuous polymer film on particle surfaces and within pores. This process increases the effective contact area for gas–solid–liquid multiphase reactions and enhances oxygen transport, pyrolysis-product migration, and interfacial reactions at the coal/PU interface. Meanwhile, molten PU fills the voids between coal particles, reducing the internal pore space and forming a denser continuous phase with improved thermal conductivity. This improves heat-transfer efficiency within the system and reduces local cold zones caused by poor contact in pure coal samples, allowing the coal to heat more uniformly and rapidly. As the temperature increases, high PU contents (>16.67%) promote the formation of a ceramic-like bridging phase between coal particles, resulting in a dense coked mass after cooling (Figure 9). During the reaction, this viscous molten phase, or initially formed coked network, may temporarily restrict the escape of some macromolecular products, prolonging their residence time in the high-temperature zone and promoting deep cracking or secondary reactions that generate more small-molecule combustible gases, such as CO and C_2H_4. In addition, the molten phase may act as a microreactor for the coupling and rearrangement of free radicals and active intermediates, thereby promoting pathways such as methyl–radical coupling to form ethane.

(2) Medium-temperature pyrolysis (250–350 °C). The ether bonds (-C-O-C-) and urethane bonds (-NH-COO-) in PU have relatively low bond energies and cleave within the range of 250–350 °C. This decomposition directly releases large amounts of small-molecule combustible gases, including CO, C_2H_4, and C_2H_6. These gases can undergo gas-phase oxidation with oxygen at relatively low temperatures and release additional heat. This heat acts as an external heat source that compensates for the limited heat release from coal oxidation at low temperatures, enabling the mixed system to reach the heat-release rate required for a self-sustaining reaction at a lower overall temperature. This mechanism directly explains the systematic decrease in CPT (Table 4). PU pyrolysis not only produces combustible gases but also generates highly reactive oxygen-containing radicals, such as R-O·, alkyl radicals, and isocyanate-derived radicals. These exogenous radicals can attack relatively stable aliphatic side chains and bridge bonds in the coal macromolecular structure, causing coal molecules to

cleave at temperatures lower than their normal pyrolysis temperature and generating new coal-derived radicals. In this sense, PU acts as a promoter for the chain reactions involved in coal oxidation and pyrolysis, substantially reducing the activation energy of the initial coal reaction and leading to earlier release of products such as C_2H_4 and C_2H_6.

(3) High-temperature coking (>350 °C). During high-temperature coking, PU pyrolysis and coal pyrolysis compete for hydrogen radicals (H·), which are key active species in the system. This competition strongly modifies the final gas-product distribution. For CH_4 generation, the key chain-termination step, $\cdot CH_3 + H\cdot \rightarrow CH_4$, is suppressed because H· is extensively consumed by PU-derived radicals. As a result, CH_4 production decreases as the PU content increases (Figure 4). In contrast, for C_2 hydrocarbons, PU pyrolysis directly provides precursors such as ethyl radicals ($\cdot C_2H_5$). In addition, C_2 fragments produced from coal under the initiation of PU-derived radicals are more readily stabilized as C_2H_6 through hydrogen abstraction or converted to C_2H_4 through β-elimination in a radical-rich environment. This mechanism explains the sharp increase in C_2H_4 and C_2H_6 concentrations with an increasing PU content (Figures 5 and 6). It should be noted that the proposed mechanisms of hydrogen-radical competition and active-radical attack on coal molecules are mainly inferred from the final gas-product distribution and existing knowledge of PU and coal chemical structures. Because of experimental limitations, this study did not directly detect in situ radical concentrations during the reaction, for example, by electron paramagnetic resonance (EPR). Further verification using in situ radical capture and quantum chemical calculations is needed.

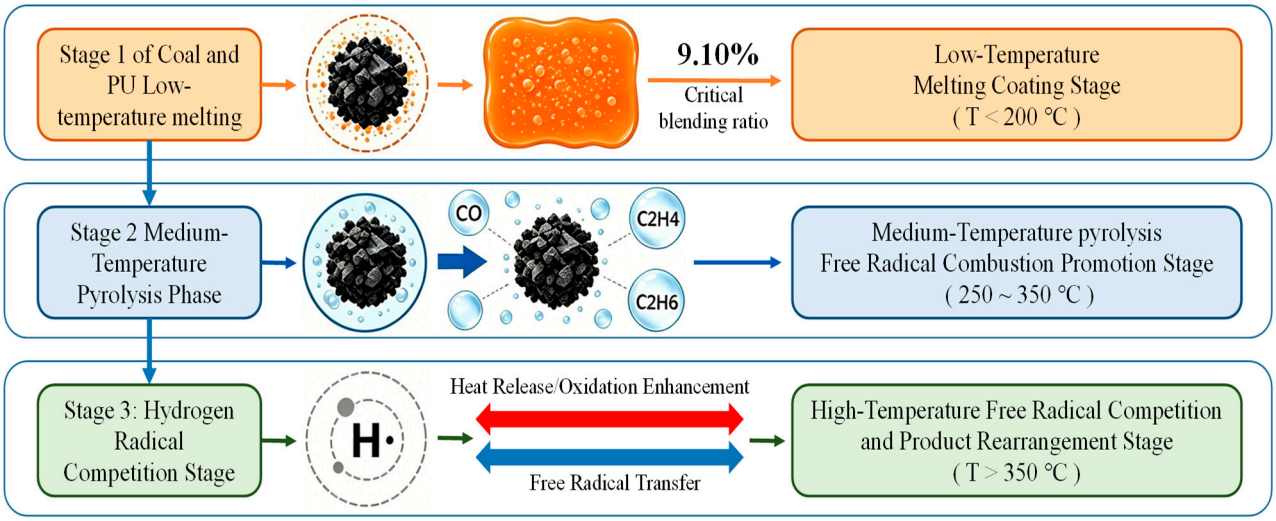


Figure 12. Schematic diagram illustrating the mechanism of the coal-PU synergistic self-ignition effect.

The decomposition of oxygen-containing functional groups in coal, including hydroxyl, carboxyl, and carbonyl groups, is the main source of CO. Amine compounds, isocyanate fragments, and other nitrogen-containing species generated during PU heating, together with the local reducing atmosphere formed by PU pyrolysis, may catalyze or synergistically participate in the decomposition of oxygen-containing functional groups in coal. This promotes CO release at lower temperatures and at higher rates (Figure 3). PU decomposition may also directly generate CO. At the same time, PU melting and coating increase the reaction interface, further accelerating this synergistic deoxygenation process.

5. Conclusions

Based on the experimental results, programmed heating tests using 2.0 kg multi-particle-size mixed samples provided a more realistic basis for analyzing the chemical reactions between coal and PU during heating. This approach also enables the direct observation of PU penetration and coating on coal particles of different sizes in the post-combustion residue.

(1) A pronounced content-dependent synergistic effect occurred during co-combustion of coal and PU. Increasing the PU content increased the release concentrations of CO, C_2H_4, and C_2H_6 and lowered their initial release temperatures, while inhibiting CH_4 generation. This inhibition was attributed to competition between PU-pyrolysis radicals and methyl radicals for hydrogen sources, which interrupts the $\cdot CH_3 + H\cdot \rightarrow CH_4$ pathway. No C_2H_2 was generated below 400 °C.

(2) The CPT decreased linearly with an increasing PU content. For every 10% increase in PU content, the CPT decreased by approximately 8.5 °C on average, and a higher PU content produced a stronger tendency toward spontaneous combustion. The mechanism is that combustible gases released by low-temperature PU pyrolysis rapidly oxidize and release heat, providing an additional heat source for coal–oxygen reactions and allowing the system to reach the self-sustaining heat-release rate at a lower temperature.

(3) Residue morphology and reaction kinetics showed consistent critical features. Glassy agglomerates appeared when the PU content exceeded 16.67%, and bulk coking occurred when the PU/coal ratio was greater than 1:10. TGA-DSC and DAEM analyses indicated that PU/coal = 1:10 was the critical point at which the synergistic effect shifted from inhibition to promotion. Under the coal conditions used in this study, the safe critical PU content is recommended to be controlled below 9.10%, and CO and C_2H_4 should be prioritized as early-warning gases. This threshold is coal-specific and was obtained for No. 3 coal from Wangzhuang Mine. It should not be directly applied to coal samples of different ranks or metamorphic degrees without systematic testing and calibration using the experimental method established in this study. Future work should conduct comparative studies on multiple coal types to develop a more general prediction model for critical parameters.

(4) Considering residue morphology and kinetic transition, the recommended safe critical PU content is $\leq$9.10%, and CO and C_2H_4 are priority early-warning gases. This threshold is based on No. 3 coal from Wangzhuang Mine and is coal-specific; targeted verification is required for other coal ranks. The synergistic effect proceeds through three stages: low-temperature melting and coating, medium-temperature pyrolysis that supplies gases and free radicals, and high-temperature radical competition. Thermodynamically, this effect decreases CPT and increases heat release. Kinetically, it changes reaction pathways and the gas-product distribution by promoting CO, C_2H_4, and C_2H_6 while inhibiting CH_4. Macroscopically, it substantially increases the spontaneous-combustion risk of coal.

Author Contributions: Conceptualization, Y.W. and B.J.; methodology, Z.P.; software, R.L.; validation, T.Y., H.Z. and Z.H.; formal analysis, Y.W.; investigation, B.J.; resources, Z.P.; data curation, Y.W.; writing—original draft preparation, R.L.; writing—review and editing, Z.H.; visualization, T.L.; supervision, T.Y.; project administration, Z.P.; funding acquisition, Y.W. All authors have read and agreed to the published version of the manuscript.

Funding: This research was funded by the Education Department of Hunan Province of China, grant number 23C0407; National College Students' Innovation and Entrepreneurship Training Program, grant number S202411528042; Hunan University Students' Innovation and Entrepreneurship Program,

grant number S202511528209X; and the study on spontaneous combustion at the No. 4 coal seam working face, grant number HX2024672644. Plus, the APC was funded by HX2024672644.

Institutional Review Board Statement: Not applicable.

Data Availability Statement: All relevant data supporting the findings of this study will be provided by the authors upon request after the publication of this article.

Acknowledgments: The authors would like to thank the editors and reviewer for their careful review of this paper.

Conflicts of Interest: Author Yu Wang were employed by Shanxi Lu'an Mining Group Co., Ltd. at the time this study was conducted. All authors declare that this employment and the funding received did not influence the study design, data collection, analysis, interpretation, writing of the article, or the decision to submit it for publication. The authors declare that the research was conducted in the absence of any commercial or financial relationships that could be construed as a potential conflict of interest.

Abbreviations

The following abbreviations are used in this manuscript:

PU	Polyurethane
CPT	Crossing Point Temperature
TGA-DSC	Thermogravimetry-Differential Scanning Calorimetry
DAEM	Distributed Activation Energy Model
EPR	Electron Paramagnetic Resonance
DTG	Derivative Thermogravimetry

References

1. Fang, Y. Research on the Impact of New Energy Development on Coal Market Consumption. *Mark. Wkly.* **2024**, *37*, 82–85. Available online: https://oversea.cnki.net/kcms2/article/abstract?v=lcmN7dc1d_P0xRzdhy4chzzAHVyTtYCKMgC21gPmYYYKlZtVOJu5CHNDcYkjoXwuBUjbQEJhIwS1ZJ1BDFOmsqAwt09W1Ojd85tdd-lv5hRXsT4rXhL6HknfS-IffMMHFtwjOjNqOV7nKEWsNsyPfZHZKFNJhKoeo8IkCSfYsmwAV8t0ZKB6_A==&uniplatform=OVERSEA&language=EN (accessed on 1 December 2025).
2. Li, D. Study on Supercritical Carbon Dioxide Displacing Coalbed Methane. Master's Thesis, Taiyuan University of Technology, Taiyuan, China, 2012. Available online: https://kns.cnki.net/verify/home?captchaType=clickWord&ident=bc397c&captchaId=cb2625e4-22b9-41cb-9038-4bd5041c49f0&returnUrl=iECBDnhr716Qd6pbb7El10nguP5Sbm9UQxpzsYxSAM-JuReIJajXtBovJQ36ss1itmBbCIWt1OZnoph3t6s-IyR0DIMIqw_HV6NZ_QdV6fRm2S8_QEZU4r0dfphP3pDf1yE4if5MLQcU9-CXhUgEKoIe3odW6Lgk73E_0xYVSmi_kguZlhoxOK1PTfJq9aZtp3nabWsB1qyNQlsHpQPwIKZZBR6fUjNtBgl-h2ZO0kgDbl5C2VVGILDLkr1ZnDHkIXRIa_5dQHr-s8oxYK61-fclq0fvSYR1nRFbpYKfXKs6lax_mTmysu4xMPOT3nb5pFHUb0UFnfsYRGlaWn91kt6sjb40k8AwFOqjvR9zAUY%3D (accessed on 1 December 2025).
3. Hou, K.; Wang, S.; Yao, S.; Niu, X.; Li, Z.; Wu, C.; Feng, G. Research Progress on the Modification of Polyurethane-based Grouting Materials for Mining. *Coal Sci. Technol.* **2022**, *50*, 28–34. [CrossRef]
4. Guo, P.; Tang, Y.; Wang, H.; Hu, S.; Zhou, J. Study on the Effect of Polyurethane on the Kinetic Characteristics of Coal Spontaneous Combustion. *Chin. J. Saf. Sci.* **2020**, *30*, 68–73. [CrossRef]
5. Ma, F.; Shang, B.; Zhang, G.; Shao, H.; Zhang, X.; Peng, L. Experiments on Controlling Roof Using Polyurethane Consolidated Coal Walls. *Coal Sci. Technol.* **1983**, *6*, 25–28. [CrossRef]
6. Wang, K.; Bai, G.; Zhang, Y.; Yu, X.; Jia, M. Research Status and Development Trends of Reactive Polymer Materials in Coal Mines. *Coal Chem. Ind.* **2022**, *45*, 129–135, 157. [CrossRef]
7. Li, B. Analysis of Accidents Involving Polymer Materials in Coal Mines. *Coal Mine Electromech.* **2020**, *41*, 62–65. [CrossRef]

8. Xu, Y.; Du, Y.; Du, B. Experimental study on the mechanism of underground fire ignition caused by the exothermic reaction of polyurethane materials used in mines. *Min. Saf. Environ. Prot.* **2019**, *46*, 29–33. Available online: https://kns.cnki.net/verify/home?captchaType=clickWord&ident=bc397c&captchaId=417497e2-842d-46b4-acfd-87aa9f2434e4&returnUrl=iECBDnhr716Qd6pbb7El10nguP5Sbm9UQxpzsYxSAM-JuReIJajXtBovJQ36ss1itmBbCIWt1OaAGVFkzY_vGTiTOug-plkE6aQFAS0308Oqbkq2GBwCbZRWFY2uyqZx6undCARNm9zLkopZDdk7h0DwNfMoYd5Y5udFFXmkzHk1JaOg1dGLKNUBtlbP979vF5pvuUzJPXCrV76SD-zYrHWCFEVuWnMYE1GdGn-hC0CSqRTm7Rd57-z9JJbfxfOqGkQQrL9AkwQ0hiOqE9Pjd6sK3dL_-82iWMPd-dOD0nA81Q3sIgGhzsFGHggEiWW1kzj8EtoD8SAI5h_NT8Oat0lJEzd05ACnhqL-ixPFapaY%3D (accessed on 1 December 2025).
9. Wang, Q.; Jin, S.; Luo, Z.; Li, Z. The Effect of Coal Metamorphism Degree on Coal Combustion Kinetic Parameters. *Saf. Environ. Eng.* **2022**, *29*, 62–70. [CrossRef]
10. Yang, P. Study on the Effect of Particle Size on the Thermokinetic Characteristics and Critical Parameters of Coal Spontaneous Combustion. *Coal Mine Saf.* **2024**, *55*, 120–129. [CrossRef]
11. Wang, H.; Tian, Y.; Li, J.; Chen, X. Experimental study on thermal effect and gas release laws of coal-polyurethane cooperative spontaneous combustion. *Sci. Rep.* **2021**, *11*, 1994. [CrossRef] [PubMed]
12. Ye, Z.; Gong, X.; Hu, M.; Shang, B. Analysis of the correlation between coal spontaneous combustion gas products and microscopic functional groups. *Coal Technol.* **2024**, *43*, 246–250. [CrossRef]
13. Tang, Y.; Guo, P. Experimental investigation on spontaneous combustion of coal affected by exothermic reaction of polyurethane in underground coal mines. *J. Therm. Anal. Calorim.* **2020**, *147*, 337–346. [CrossRef]
14. Li, T. Study on Spontaneous Combustion Kinetics and Product Generation Laws of Coal-Polyurethane Binary System. Doctoral Thesis, China University of Mining and Technology, Beijing, China, 2021. [CrossRef]
15. Wang, H.; Chen, X.; Wang, Z.; Xiang, L. Influence of Oxygen Concentration on Combustion Kinetics and Gas Products of a Polyurethane-Coal Mixture. *Fire* **2022**, *5*, 181. [CrossRef]
16. Wang, H.; Tian, Y.; Chen, X.; Li, J. Kinetic and Synergetic Effect Analysis of the Co-Combustion of Coal Blended with Polyurethane Materials. *ACS Omega* **2020**, *5*, 26005–26014. [CrossRef] [PubMed]
17. Chi, J. Application of polyurethane material spraying in underground coal mine roadways. *Energy Technol. Manag.* **2023**, *48*, 51–53. Available online: https://kns.cnki.net/verify/home?captchaType=clickWord&ident=bc397c&captchaId=6b975cf1-b56c-4d84-b5fd-20c9a10e9618&returnUrl=iECBDnhr716Qd6pbb7El10nguP5Sbm9UQxpzsYxSAM-JuReIJajXtBovJQ36ss1itmBbCIWt1OaEL9OoK0xuk2OUSmcT5WI2iWXBTlf7MjM5qHD8UAmX2BEFCauX6JSkZg_sLH6nrkV3wJcgIFPYR_I6hXETDavuFH1-vuYBNUJQDgDDeI7oAgRXS8FCSOXnGlGiPzYxUYLLBItBRrWWVYWDKUivhz37B-K2xcwwF63BOWayYXCmzTx4PkBFNE2gzFd3VOD3ICunh71FARSooj3KxpaSkUbl64SdopDzQ_aoOOljJQ0pnfb3sC8uFMgqipT5nntxTWyfgM7jqgDuaDnS3mgiYB4InzqIRMI6Ep4%3D (accessed on 1 December 2025).
18. Cheng, Y.; Lin, B.; Hao, Z.; Gao, Y.; Li, F.; Dai, H.; Yu, J. CFD simulation of two-liquid mixing uniformity of polyurethane sealing materials. *Coal Mine Saf.* **2012**, *43*, 53–56. [CrossRef]
19. Shen, J.; Yuan, N.; Ma, Y.; Zhu, J.; Jia, L. Study on low-temperature polyurethane materials for mining. *New Chem. Mater.* **2022**, *50*, 290–294. [CrossRef]
20. Liu, Y.; Li, X.; Wang, W.; Zhang, S.; Jia, L.; Zhu, F.; Yu, W. Preparation and performance of coal gangue powder/polyurethane composite grouting materials. *New Chem. Mater.* **2025**, *53*, 251–255, 265. [CrossRef]
21. Han, X.; Liu, Q.; Zhou, K. Preparation and performance of EG/DMMP composite-modified polyurethane grouting materials. *Saf. Environ. Eng.* **2024**, *31*, 25–33. [CrossRef]
22. Liu, Q.; Liu, C.; Zhou, K. Experimental study on polyurethane grouting materials for coal mine safety protection. *Saf. Environ. Eng.* **2021**, *28*, 65–74. [CrossRef]
23. Zhan, M.; Sun, L.; Cheng, W.; Lv, X.; Shi, Q.; Huang, Q.; Wang, H. Experimental study on coal seam moisturizing inhibitor and mechanism of preventing coal spontaneous combustion. *Energy* **2024**, *291*, 130312. [CrossRef]
24. Jiang, H.; Liu, X.; Zou, Y.; Zhou, Z.; Huang, X.; Tang, G. Preparation and flame-retardant performance of rigid polyurethane foam/ammonium polyphosphate composites. *Plast. Ind.* **2019**, *47*, 89–93. Available online: https://kns.cnki.net/verify/home?captchaType=clickWord&ident=bc397c&captchaId=bbed0145-1b60-4cb0-979e-dcfe50d76de4&returnUrl=iECBDnhr716Qd6pbb7El10nguP5Sbm9UQxpzsYxSAM-JuReIJajXtBovJQ36ss1itmBbCIWt1Ob55-P9nnDIOJ8B2PW8wUumnvgpcHHunCvEUrMkk--Y5laH1DtqC4PdYCzd2hGKxOLMf4Zr5apDw-GGfQNlIi_Vf3HU45S2NIvhJri4gSKuuSuv2s_QHrOF4MuNk53o97RYAD8z8_dOpiSEy-Of9cuYaaAgkP7xdVgE3rW20hL2_GzHRUb1TE6wWsaSLMHP4jz3m98q06DtEcqirysTkB9G3aRY5aE_2e7bsDbdE5l8tT0NpPTNaeJioPJlQOB52Tzzwg8JJhedIEEhp365VE8tutiM-BaumMs%3D (accessed on 1 December 2025).
25. Zhang, L.; Wu, W.; Wei, J.; Bian, Y.; Luo, H. Preparation of foamed gel for preventing spontaneous combustion of coal. *Fuel* **2021**, *300*, 121024. [CrossRef]

26. Yang, Z.; Xue, R.; Wang, J.; Lan, Z. Development and performance of modified polyurethane rapid grouting water-plugging materials. *Coal Geol. Explor.* **2020**, *48*, 134–140. Available online: https://kns.cnki.net/verify/home?captchaType=clickWord&ident=bc397c&captchaId=135c20e8-ca8e-4c9f-9054-6d3f7c22b244&returnUrl=iECBDnhr716Qd6pbb7El10nguP5Sbm9UQxpzsYxSAM-JuReIJajXtBovJQ36ss1itmBbCIWt1OaRM_6cjiJnTTvaeIe24wJEcpdhP83TMyoHGgfNsZWUVH2xjthBln9BpSQMQhnFchbVPmklMr0o1_cQc7CtHnrj6qYBZu6wT6HyAg57lVchhuS5xfNmRP3DDGSFX9IHlPNHR9w-7vlykSKwA2G3TO7apYRd4xhH0ZFpmQIVu2ttKjPYy1670xkVKUzeCblSfHl6-ziaT6lqxS1fZoJ7hK3_AAqFnsozbcK1xLbnSj53-wqiCLc6BraNAZU3oT1GnxRDpS4-WSaAfHKFy5Pwb52r9FjkDIb2Z9g%3D (accessed on 1 December 2025).
27. Gao, M.; Feng, T.; Sun, C.; Zhang, C. Microencapsulated diatomite-supported flame retardant for modified mining polyurethane foam. *Eng. Plast. Appl.* **2024**, *52*, 41–47. Available online: https://kns.cnki.net/verify/home?captchaType=clickWord&ident=bc397c&captchaId=4e274ba6-a67d-45bc-a1f6-4c0135393f48&returnUrl=iECBDnhr716Qd6pbb7El10nguP5Sbm9UQxpzsYxSAM-JuReIJajXtBovJQ36ss1itmBbCIWt1OaAGoiVML7FnR1RsROy-BFH-jVHtGQBeGk7LjQ-p9johyX8r-iamo-_995mf8IBsGOjx0O7sAGNgAe5O_-MHa9he7iouP2wqUueOkyZcKPoKy3ylafMz1ml1YIEyAzFJhUK3BdZpc5SX2LZ75_I5tVvGejFrxXnmTttSGPefiQ2VvC-YsxkBnA3QaSsMIBoP78d4cuEzwFhEgPj4JIBPVLjphTJrBQp7jNHeKzcYwz7bx0mYXHdLCncIpJE_J7O0pQ-D30moN7Gz-oUjImKx0cM-wyBK-06ssS4%3D (accessed on 1 December 2025).
28. Wang, B. Causes and control of disasters induced by heat release from mining polyurethane materials. *Mod. Ind. Econ. Inf.* **2022**, *12*, 265–267. [CrossRef]
29. Yang, S.; Dong, W.; Zhou, X.; Xu, X. Flame retardancy and reinforcement performance of mining polyurethane grouting materials. *Chin. J. Saf. Sci.* **2012**, *22*, 48–53. [CrossRef]
30. Cheng, J.; Shen, W. Development of flame-retardant polyurethane filling materials for underground coal mines. *Coal Min. Technol.* **2012**, *17*, 14–16, 34. [CrossRef]
31. Wang, L.; Tawiah, B.; Shi, Y.; Cai, S.; Rao, X.; Liu, C.; Yang, Y.; Yang, F. Highly Effective Flame-Retardant Rigid Polyurethane Foams: Fabrication and Applications in Inhibition of Coal Combustion. *Polymers* **2019**, *11*, 1776. [CrossRef] [PubMed]
32. Ma, Y.; Du, W.; Wu, B.; Wu, H.; Huang, Q. Experimental Study on the Combustion Characteristics of Polyurethane Under High Pressure and Low Oxygen Environment. *Fire Technol.* **2019**, *55*, 915–934. [CrossRef]
33. Chen, H.; Wang, J.; Zong, R. Effect of sample size on combustion performance of thermoplastic polyurethane. *Fire Sci. Technol.* **2021**, *30*, 1–8. Available online: https://oversea.cnki.net/kcms2/article/abstract?v=lcmN7dc1d_MOQDTgULcbZfnLC9XBtV3hsmhVpbMlB5Nq3v_j1d61HC2qM83fBJPsxy96BAb52MLb0WYgByWZyxl-rLxKiRDCHd7d1twyIYB9wyS7dKBzSMxGzlAYvzac0mkM8bdvI-JIvtL0uU2OYgTpxxnGHGdxmmkR_NFlZc5vLy9Y5fChJw==&uniplatform=OVERSEA&language=EN (accessed on 1 December 2025).
34. Ren, S.; Ren, H.; Ji, Y. Fire causes and fire prevention of polyurethane foam plastics during production and storage. *Fire Technol. Prod. Inf.* **2003**, *10*, 26–29. Available online: https://kns.cnki.net/verify/home?captchaType=clickWord&ident=bc397c&captchaId=8a899688-bddd-43a8-b524-2138c867526d&returnUrl=iECBDnhr716Qd6pbb7El10nguP5Sbm9UQxpzsYxSAM-JuReIJajXtBovJQ36ss1itmBbCIWt1Oa55KDOBrnHylWoSmquOk-BgcQZ4oQ4DhVdTlXzB1Vd28GcFzPNnzRDJa2qwFxacjhGz9x-1dSdJEi2kOg9O5_CcTzAFFexEuhEwfoP6AsfCwVDux8Ujx9ur-QCDorCtc7RQenpUjsaWiplsk4NrGLnNIiaxLDfc-FencyRHmG4CFLBqpXKBlm8soA1iOR0XyhJf_9w83PMuHJ7dOrP3xX578fNQ_H86yVp6GI9tj250c_8dK7BNsST9ScRyT8caxnv3GzVQ3CqJQoeSU-aaopVqN (accessed on 1 December 2025).
35. Zhang, Z. Preparation and fireproof performance of safe polyurethane reinforcement materials. *Coal Sci. Technol.* **2020**, *48*, 148–152. [CrossRef]
36. Zhang, P.; Xin, H.; Bai, G.; Ju, S.; Qi, X.; Dong, Z.; Wang, D. Study on gas release behavior and multi-level early warning mechanism of polyurethane and coal co-combustion. *Fire Saf. J.* **2025**, *157*, 104481. [CrossRef]
37. Li, Y.; Chen, G.; Wang, Y.; Yu, X. Research progress on modification of polyurethane grouting materials for coal mines. *Coal Qual. Technol.* **2025**, *40*, 9–15. Available online: https://oversea.cnki.net/kcms2/article/abstract?v=lcmN7dc1d_OxCE-PMTaJA6jHUH_nuzZjNdTV7M3mJP5KtCK8u8xlHWwJefRQ-MUxxC5PjCSWgPSKXLz4LDwAR_t9h9Ope2x8LxoiN5N7NXRRZ8Ywh7aaTs1G0xcLMnvZfaSIbqycbT-TcqawVzfnIpAuvGvjHnpO7qWPOE2FQ3needxsG_275w==&uniplatform=OVERSEA&language=EN (accessed on 1 December 2025).
38. Lu, Q.W.; Hernandez-Hernandez, M.E.; Macosko, C.W. Explaining the abnormally high flow activation energy of thermoplastic polyurethanes. *Polymer* **2003**, *44*, 3309–3318. [CrossRef]
39. Dzunuzovic, J.V.; Stefanovic, I.S.; Dzunuzovic, E.S.; Marega, C. Thermal degradation kinetics of urethane and urea linkages of waterborne polyurethanes. *Phys. Chem.* **2024**, *2*, 405–408. [CrossRef]

Disclaimer/Publisher's Note: The statements, opinions and data contained in all publications are solely those of the individual author(s) and contributor(s) and not of MDPI and/or the editor(s). MDPI and/or the editor(s) disclaim responsibility for any injury to people or property resulting from any ideas, methods, instructions or products referred to in the content.